Composite Structures 241 (2020) 112088

Contents lists available at ScienceDirect

Composite Structures

journal homepage: www.elsevier.com/locate/compstruct

Comparison and experimental verification of simplified one-dimensional linear elastic models of multilayer sandwich beams

Paweł Szeptyński*

Division of Structural Mechanics and Material Mechanics, Faculty of Civil Engineering, Cracow University of Technology, Poland

ARTICLE INFO

Keywords:
Composite beams
Laminated beams
Sandwich beams
CLT
Linear elasticity

ABSTRACT

Three analytical one-dimensional linear elastic models of composite laminated beams are considered – composite Bernoulli-Euler beam (BE), composite Timoshenko beam (T) and multilayer sandwich beam model (MS). They are compared with results obtained via finite element method for a two-dimensional model in plane stress state. Overall system stiffness is verified with experimental data obtained for two statical configurations – three-point bending and four-point bending. The first configuration concerned 8 types of three-panel cross-laminated timber (CLT) beams accounting for various materials and thickness of timber panels as well as various materials and thickness of adhesive layer, while the second one concerned 5 types of two-panel aluminium laminated beams accounting for different thickness of adhesive layer. Simplified multilayer sandwich model is found to be in good accordance with FEA results and with experimental data, while simple BE and T models are shown to provide erroneous estimates.

1. Introduction

Composites enable considerable flexibility in design of functionality of the structure as a whole as well as concerning each composite structural element separately. Composite structures make also more efficient use of available resources by appropriate stress distribution accounting for different bearing capacities of their components. Some of such solutions are particularly simple in serial production, e.g. laminated (gluelam) beams or Cross Laminated Timber (CLT) beams consisting of multiple layers of relatively rigid panels and more compliant adhesive. The use of adhesives of higher flexibility was reported to result in even more efficient use of material's bearing capacity [1–3]. Construction of large structures consisting of multiple composite elements require appropriate simplified models in order to carry out calculations efficiently. For a certain class of design problems restrictions on admissible deformation result in limiting the material behaviour regime to sole linear elasticity (small strains and displacements) – e.g. in case of framework structures in civil engineering. Linear elastic models, due to principle of superposition, enable direct element design methods. They may be also used in order to determine element stiffness matrix for more complex structural analysis with the use of Finite Element Method if only proper nodal displacement compatibility is provided.

The aim of this article is a preliminary comparison of simplified linear elastic one-dimensinal models [4] of composite beams in order to verify their applicability in the design and analysis of complex composite bar structures (frameworks, trusses etc.). Among such models one may distinguish the Bernoulli-Euler beam, Timoshenko beam [5] and sandwich beam theories [6]. The classical theories may be easily generalized in order to account for a composite structure of the beam's cross-section. Many alternative approaches were used in modelling the sandwich beams and plates, accounting for shear deformation determined by an assumption of various shear stress distribution functions [7–12]. The present article deals with a model of a multilayer sandwich beam consisting of multiple bending layers (Bernoulli-Euler beam) and shear layers (simple shear deformation) placed in an alternating way – it will be referred to as MS beam. It is compared with composite Bernoulli-Euler (BE) and composite Timoshenko (T) beams as well as with the solution of the two-dimensional solution of plane stress state problem of linear theory of elasticity obtained via Finite Element Analysis

* Address at: Cracow University of Technology, Faculty of Civil Engineering, Institute of Structural Mechanics, ul. Warszawska 24, 31-155 Kraków, Poland.
E-mail address: pszeptynski@pk.edu.pl.

https://doi.org/10.1016/j.compstruct.2020.112088
Received 19 June 2019; Received in revised form 10 October 2019; Accepted 20 February 2020
Available online 22 February 2020

(FEA). All results are verified with the experimental data on – in total – 13 beam types in two statics configurations: three-point bending and four-point bending.

2. Compared models

2.1. Composite Bernoulli-Euler beam

Fundamental assumption of a composite Bernoulli-Euler (BE) model is the Bernoulli hypothesis on plane cross-sections stating that there is no deplanation and orthogonality of cross-section to the beam's axis is preserved during deformation. This results in linear distribution of linear strain which – in case of composite cross-section – yields a non-linear distribution of normal stress. The governing equations of BE model is a well-known fourth order ordinary differential equation (ODE):

$$\frac{d^2}{dx^2}\left(D_b\frac{d^2w}{dx^2}\right)=q(x) \tag{1}$$

where:

$$D_b=\iint_A z^2\cdot E(z)\mathrm{d}A, \tag{2}$$

is the flexural rigidity (which may be considered a function of cross-section), $q(x)$ is the load distribution along beam length, $E(z)$ is the through-the-thickness distribution of Young modulus in a composite cross-section, and z is the distance from the elastic weighted centroid found in any coordinate system aligned with beam axis and axis of bending as:

$$Z_O=\frac{S_b}{A_b},\ \text{where}\ \ A_b=\iint_A E(z)\mathrm{d}A,\quad S_b=\iint_A z\cdot E(z)\mathrm{d}A. \tag{3}$$

Normal stress distribution in each point is proportional to the linear strain which $E(z)$ being the proportionality factor:

$$\sigma(x,z)=-\frac{d^2w}{dx^2}z\ E(z) \tag{4}$$

Shear stress distribution may be approximated with the use of Zhuravsky theory [13,14] as:

$$\bar{\tau}=\int_z^{Z_0}\frac{\mathrm{d}\sigma(x)}{\mathrm{d}x}\mathrm{d}z \tag{5}$$

Analytical formulae for the above quantities may be easily computed for any piecewise constant distribution of $E(z)$ respective for a laminated beam of layers of finite thickness.

2.2. Composite Timoshenko beam

The model of Timoshenko [5] releases the assumption on the orthogonality of plane cross-section to the deformed axis. The angle of rotation about the axis of bending ϕ provides an additional degree of freedom. The model is governed by a system of ODEs:

$$\frac{\mathrm{d}^2}{\mathrm{d}x^2}\left(D_b\frac{\mathrm{d}\phi}{\mathrm{d}x}\right)=q, \tag{6}$$

$$\frac{\mathrm{d}w}{\mathrm{d}x}=\phi-\frac{1}{\kappa D_s}\frac{\mathrm{d}}{\mathrm{d}x}\left(D_b\frac{\mathrm{d}\phi}{\mathrm{d}x}\right), \tag{7}$$

where flexural rigidity D_b is defined as above, and shear rigidity is given as:

$$D_s=\iint_A G(z)\mathrm{d}A \tag{8}$$

where $G(z)$ is the through-the-thickness distribution of Kirchhoff modulus in a composite cross-section. Stress distribution is assumed to be the same as in case of BE model. Multiple estimates of the shear-correction factor for a Timoshenko beam were made [15–20]. The one which may be easily extended for the case of composite cross-section is based on comparison of elastic strain energy due to shearing according to Timoshenko model with its estimate based on Zhuravsky theory [13] of shear stress distribution. Transverse (shear) force in a composite Timoshenko beam may be defined as:

$$\begin{aligned}Q&=\kappa\iint_A\tau_{xz}dA=\kappa\iint_A 2G(z)\varepsilon_{xz}dA=\kappa\iint_A G(z)\left(\frac{dw}{dx}-\phi\right)dA\\&=\kappa D_s\left(\frac{dw}{dx}-\phi\right)\end{aligned} \tag{9}$$

Then the elastic strain energy due to shearing may be written down as follows:

$$\begin{aligned}U_s&=\iiint_V 2\tau_{xz}\varepsilon_{xz}dV=\iiint_V 4G(z)\varepsilon_{xz}^2dV\\&=\int_{x=0}^{L}\left[\kappa\iint_A G(z)\left(\frac{dw}{dx}-\phi\right)^2dA\right]dx=\int_{x=0}^{L}\left[\kappa D_s\left(\frac{dw}{dx}-\phi\right)^2\right]dx\\&=\int_{x=0}^{L}\left[\frac{1}{\kappa D_s}\left(\kappa D_s\left(\frac{dw}{dx}-\phi\right)\right)^2\right]dx=\frac{1}{\kappa}\int_{x=0}^{L}\frac{Q^2}{D_s}dx\end{aligned}$$

According to the Zhuravski estimate, one may write:

$$\begin{aligned}U_s&\approx\iiint_V 2\bar{\tau}_{xz}\bar{\varepsilon}_{xz}dV=\int_{x=0}^{L}\left[\iint_A\frac{\bar{\tau}_{xz}^2}{G(z)}dA\right]dx\\&=\int_{x=0}^{L}\left[\frac{1}{G(z)}\iint_A\left(\int_{\zeta=z}^{Z_0}\frac{\mathrm{d}\sigma(x)}{\mathrm{d}x}\mathrm{d}\zeta\right)^2dA\right]dx=\int_{x=0}^{L}\left[\iint_A\frac{Q^2s^2(z)}{G(z)D_b^2}dA\right]dx\\&=\int_{x=0}^{L}\left[\frac{Q^2}{D_s}\left(\frac{D_s}{D_b^2}\underbrace{\iint_A\frac{s^2(z)}{G(z)}dA}_{\alpha}\right)\right]dx=\alpha\int_{x=0}^{L}\frac{Q^2}{D_s}dx\end{aligned}$$

what enables us to write:

$$\kappa=\frac{1}{\alpha}=\left(\frac{D_s}{D_b^2}\iint_A\frac{s^2(z)}{G(z)}dA\right)^{-1} \tag{10}$$

where $s(z)$ is the elastic weighted statical moment of the above-z part of the cross-section about the axis passing through the weighted centroid. This approximation is far from being precise, as in the derivation of governing equations of the Timoshenko beam parameter is once used as a scaling factor providing actual value of integral of the stress (strain) distribution in a cross-section, namely the value of transverse force which is a linear function of stress and for the second time it is used as a scaling factor providing actual value of an integral of strain energy density which is a quadratic function of stress. This scaling factor in both of those case will be in general different.

2.3. Simplified multilayer sandwich beam model

Proposition on another one-dimensional linear elastic model may be briefly described as a system of multiple bent and sheared layers placed in an alternating way. The bending layers are assumed to be homogeneous Bernoulli-Euler beams, while the shear (adhesive) layers are assumed to be in simple shear state. Equilibrium equations may we written down as follows (See Fig. 1):

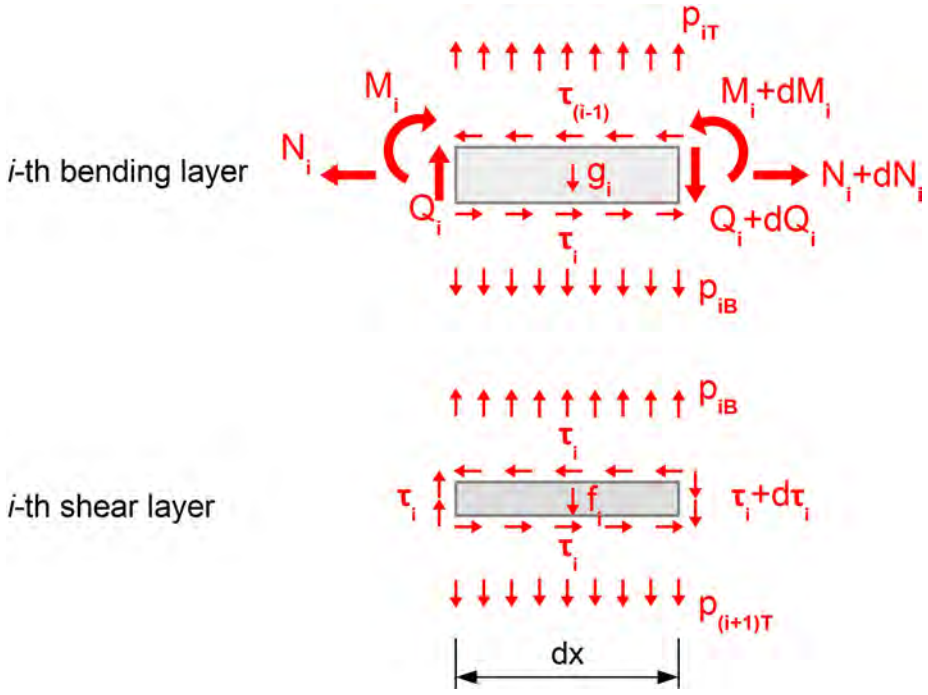

Fig. 1. Equilibrium of bending and shear layers.

Axial direction

$$\frac{dN_1}{dx} + b\tau_1 = 0 \tag{11a}$$

$$\frac{dN_i}{dx} - b\tau_{(i-1)} + b\tau_i = 0,\ i = 2,\ \cdots,N \tag{11b}$$

$$\frac{dN_{(N+1)}}{dx} - b\tau_{N,T} = 0 \tag{11c}$$

Transverse direction:

$$\frac{dQ_1}{dx} + q + bp_{1,B} + h_1 g_1 = 0 \tag{12a}$$

$$\frac{dQ_i}{dx} - bp_{i,T} + bp_{i,B} + h_i g_i = 0,\ i = 2,\ \cdots,N \tag{12b}$$

$$\frac{dQ_{(N+1)}}{dx} - bp_{(N+1),T} + h_{(N+1)} g_{(N+1)} = 0 \tag{12c}$$

Moment equilibrium:

$$\frac{dM_1}{dx} - Q_1 + \tau_1 \frac{bh_1}{2} = 0 \tag{13a}$$

$$\frac{dM_i}{dx} - Q_i + (\tau_{(i-1)} + \tau_i)\frac{bh_i}{2} = 0,\ i = 2,\ \cdots,N \tag{13b}$$

$$\frac{dM_{(N+1)}}{dx} - Q_{(N+1)} + \tau_N \frac{bh_{(N+1)}}{2} = 0 \tag{13c}$$

where M_i, Q_i, N_i are bending moment, transverse force and axial force in i-th bending layer respectively, $p_{i,T}$, $p_{i,B}$ are the through-the-thickness normal stress at top and bottom surface of the i-th bending layer respectively, b is the constant beam's width, h_i is the thickness of i-th bending layer and τ_i is the shear stress in an adhesive layer between

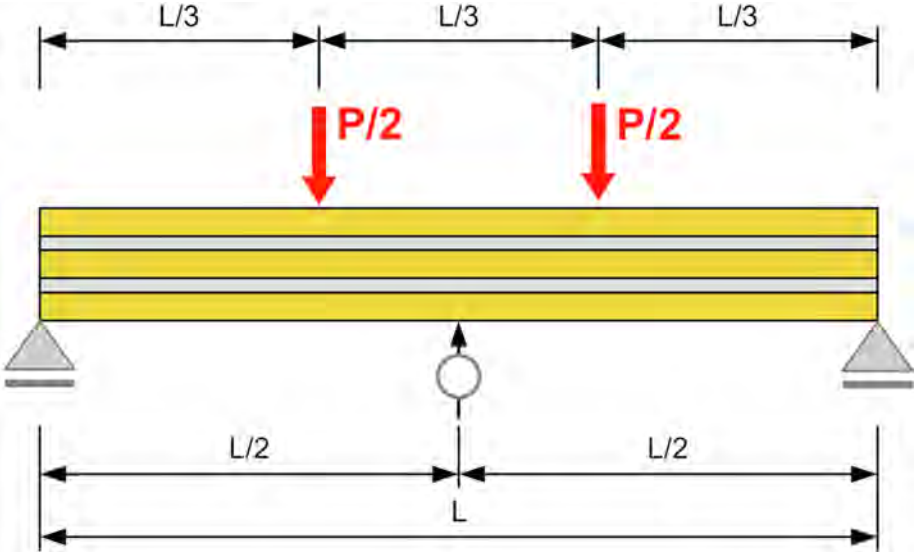

Fig. 2. Four-point bending of three-layer CLT beam. Statical configuration and location of gauge.

bending layers i and $(i+1)$. External load is given by surface traction q at top surface of the topmost bending layer and by the distribution of body forces g_i in bending layers andf_i in shear layers.

Let us combine the equilibrium equations for transverse direction and moment equilibrium equations and introduce constitutive relations of the form:

$$\frac{du_i}{dx} = \frac{N_i}{E_i A_i}, \frac{d^2w}{dx^2} = -\frac{M_i}{E_i I_i}, \tag{14}$$

where E_i, A_i, $I_i$are the Young modulus, cross-section area and cross-section second moment of area of the i-th bending layer. Please note, that the deflection is common for all bending layers. Then, summing up all the combined equilibrium equations for transverse forces and moment, gives us following system of governing equations:

$$E_1 A_1 \frac{d^2u_1}{dx^2} + b\tau_1 = 0 \tag{15}$$

$$E_i A_i \frac{d^2u_i}{dx^2} - b\tau_{(i-1)} + b\tau_{i,} = 0,\ i = 2,\ \cdots,N \tag{16}$$

$$E_{(N+1)} A_{(N+1)} \frac{d^2u_{(N+1)}}{dx^2} - b\tau_N = 0 \tag{17}$$

$$\sum_{k=1}^{N+1} [E_k I_k] \frac{d^4w}{dx^4} = q + \sum_{k=1}^{N+1} [h_k g_k] + \frac{b}{2} \sum_{i=1}^{N} \left[(h_i + h_{(i+1)}) \frac{d\tau_i}{dx} \right] + b \sum_{i=1}^{N} [p_{i,B} - p_{(i+1),T}] \tag{18}$$

The through-the-thickness normal stress may be ousted by an account for the equilibrium equations of the shear layers:

$$b(p_{i,B} - p_{(i+1),T}) = bt_i \frac{d\tau_i}{dx} + t_i f_i \tag{19}$$

Finally, we may express the shear stress by the displacement functions. Kinematics of the shear layer is analogous as in shear layers of classical lap joint models (i.e. [21–24]). It is assumed that the longitudinal displacement of points at interface of the shear layer with neighbouring bending layer is due to elongation of the bending layer and its rotation about central axis:

$$u_{i,B} = u_i - \frac{h_i}{2} \frac{dw}{dx} \tag{20}$$

$$u_{(i+i),T} = u_{(i+1)} + \frac{h_{(i+1)}}{2} \frac{dw}{dx} \tag{21}$$

It is assumed that the longitudinal displacement in shear layer changes linearly between those boundary values, resulting in constant shear strain and shear stress in the layer:

$$\tau_i = \frac{G_i}{t_i} \left[\left(u_{(i+1)} + \frac{h_{(i+1)}}{2} \frac{dw}{dx} \right) - \left(u_i - \frac{h_i}{2} \frac{dw}{dx} \right) \right] = \frac{G_i}{t_i} \left[(u_{(i+1)} - u_i) + \left(\frac{h_i}{2} + \frac{h_{(i+1)}}{2} \right) \frac{dw}{dx} \right],\ i = 1,\ \cdots,N \tag{22}$$

Let's substitute the above results in the Eqs. (15) to (18). After simple rearrangements, we obtain the final form of the governing equations:

$$E_1 A_1 \frac{d^2u_1}{dx^2} + \frac{b}{t_1} G_1 \left[(u_2 - u_1) + \left(\frac{h_2}{2} + \frac{h_1}{2} \right) \frac{dw}{dx} \right] = 0 \tag{23}$$

$$E_i A_i \frac{d^2u_i}{dx^2} - \frac{b}{t_{i-1}} G_{i-1} \left[(u_i - u_{i-1}) + \left(\frac{h_i}{2} + \frac{h_{i-1}}{2} \right) \frac{dw}{dx} \right] + \frac{b}{t_i} G_i \left[(u_{i+1} - u_i) + \left(\frac{h_{i+1}}{2} + \frac{h_i}{2} \right) \frac{dw}{dx} \right] = 0,\ i = 2,\ \cdots,N \tag{24}$$

$$E_{(N+1)} A_{(N+1)} \frac{d^2u_{(N+1)}}{dx^2} - \frac{b}{t_N} G_N \left[(u_{N+1} - u_N) + \left(\frac{h_{N+1}}{2} + \frac{h_N}{2} \right) \frac{dw}{dx} \right] = 0 \tag{25}$$

$$\sum_{k=1}^{N+1} [E_k I_k] \frac{d^4w}{dx^4} = q + \sum_{k=1}^{N+1} [h_k g_k] + \sum_{i=1}^{N} [t_i f_i] + \frac{b}{2} \sum_{i=1}^{N} \left[(h_i + h_{(i+1)} + 2t_i) \frac{G_i}{t_i} \left[\left(\frac{du_{(i+1)}}{dx} - \frac{du_i}{dx} \right) + \left(\frac{h_i}{2} + \frac{h_{(i+1)}}{2} \right) \frac{d^2w}{dx^2} \right] \right] \tag{26}$$

This is a fourth order system of N + 2 ordinary differential equations for N + 2 displacement functions: N + 1 longitudinal displacements of bending layers and common deflection of all bending layers. They constitute a multi-point boundary value problem. Boundary conditions should be formulated with care. Transverse deflection constraints may be accounted for in the same way as in case of classical BE model. It must be noted that edge longitudinal displacements of each panel may be in general different and they should be defined separately. In particular symmetry of a system enable simple determining of the boundary conditions. Static boundary conditions (edge point loads) may be accounted for by proper definition of cross-sectional forces.

Total cross-sectional axial force:

$$N(x) = \sum_{k=1}^{N+1} \int_{-\frac{h_i}{2}}^{\frac{h_i}{2}} [\sigma_k] dz_k = \sum_{k=1}^{N+1} E_k A_k \frac{du_k}{dx} \tag{27}$$

Total cross-sectional transverse force:

$$Q(x) = \sum_{k=1}^{N+1} Q_k + \sum_{i=1}^{N} bt_i \tau_i = \sum_{k=1}^{N+1} \frac{dM_i}{dx} + \frac{b}{2} \sum_{i=1}^{N} (h_i + h_{i+1} + 2t_i)\tau_i = -\sum_{k=1}^{N+1} [E_k I_k] \frac{d^3w}{dx^3} + \frac{b}{2} \sum_{i=1}^{N} (h_i + h_{i+1} + 2t_i) \frac{G_i}{t_i} \left[(u_{(i+1)} - u_i) + \left(\frac{h_i}{2} + \frac{h_{(i+1)}}{2} \right) \frac{dw}{dx} \right] \tag{28}$$

Speaking of total cross-sectional bending moment is perhaps irrelevant since it may be calculated as a moment of stress resultants about any point P:

$$M_P(x) = \sum_{k=1}^{N+1} \int_{-\frac{h_i}{2}}^{\frac{h_i}{2}} [\sigma_k \cdot ((z_{Ok} + z_k) - Z_P)] dz_k \tag{29}$$

None single point of particular meaning in a cross-section can be distinguished. From the statical point of view this should be the point of a central axis of system of axial forces (no moment due to axial forces) – yet, since they may vary along beam's axis, such a point would be different in each cross-sections. In fact, edge cross-sectional moment could be most easily applied rather in the form of a system of axial forces applied to the panels instead of point moment (necessarily equal for all of panels).

Distribution of normal stress within a single bending layer is the same as in classical BE theory:

$$\sigma_i(z_i) = E \left(\frac{du_i}{dx} - \frac{d^2w}{dx^2} z_i \right) \tag{30}$$

Distribution of shear stress in a bending layer may be estimated as in the Zhuravsky theory, accounting for additional shear stress at interface with shear layers:

$$\tau_{i,p}(z_i) = \tau_{i-1} - \int_{-\frac{h_i}{2}}^{z_i} \left[E_i \left(\frac{d^2u_i}{dx^2} - \frac{d^3w}{dx^3} \zeta \right) \right] d\zeta \tag{31}$$

Transverse normal strain at interfaces is given be recurrence formulae:

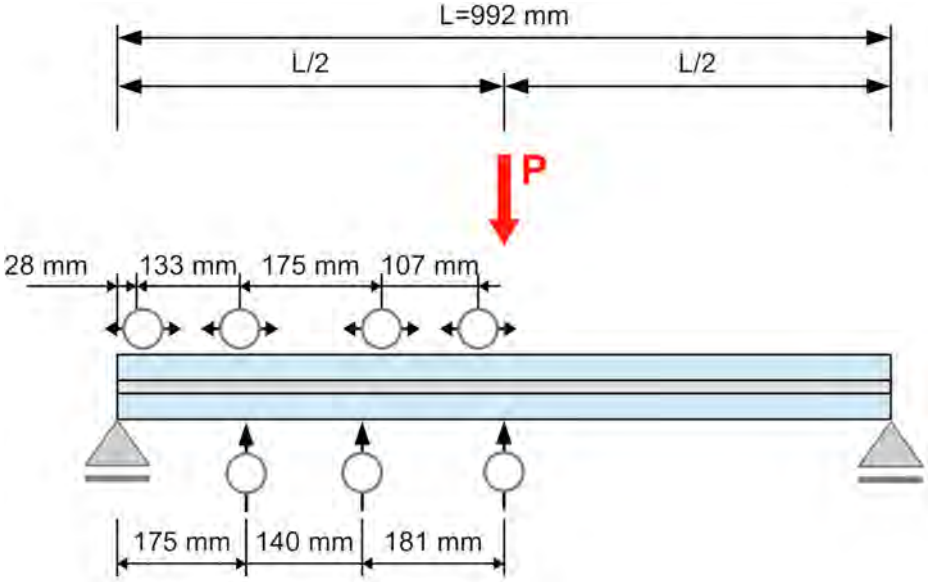

Fig. 3. Three-point bending of two-layer aluminium beam. Statical configuration and location of gauges.

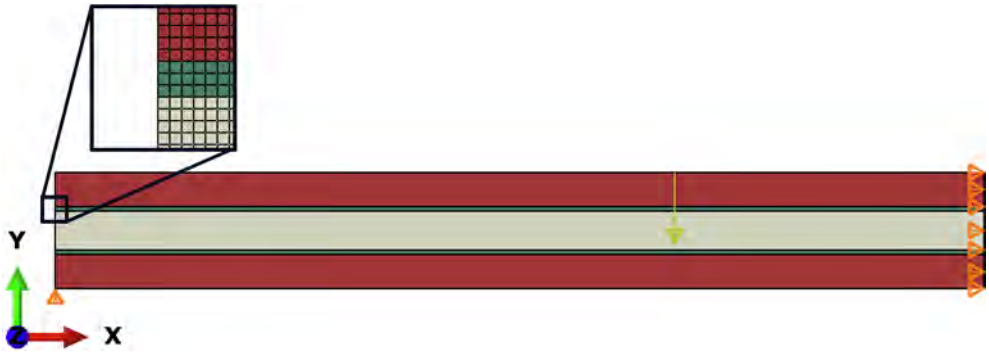

Fig. 4. Finite Element Method model of the CLT beam.

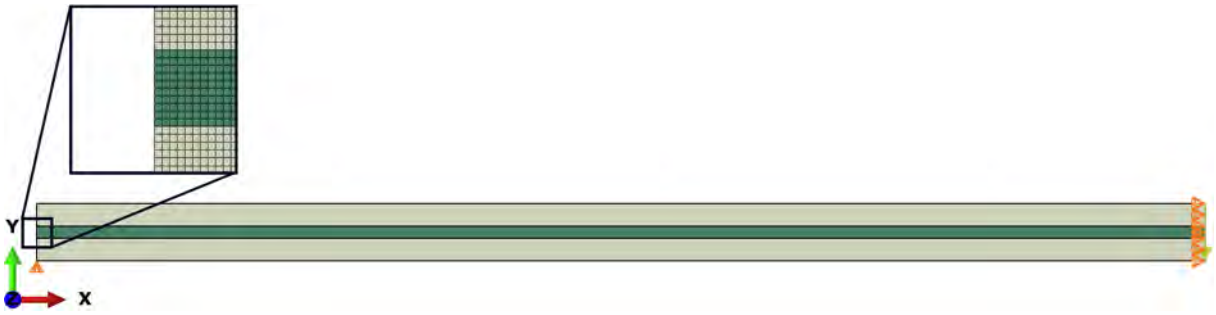

Fig. 5. Finite Element Method model of the ALU beam.

$$p_{1,B} = \frac{1}{b}\left[E_1 I_1 \frac{d^4 w}{dx^4} - q - h_1 g_1 - \frac{d\tau_1}{dx}\frac{bh_1}{2}\right], \tag{32a}$$

$$p_{(i+1),T} = p_{iB} - t_i \frac{d\tau_i}{dx} + \frac{t_i}{b} f_i,\ i = 1,\ \cdots, N, \tag{32b}$$

$$p_{i,B} = \frac{1}{b}\left[E_i I_i \frac{d^4 w}{dx^4} + b p_{i,T} - h_i g_i - \left(\frac{d\tau_{(i-1)}}{dx} + \frac{d\tau_i}{dx}\right)\frac{bh_i}{2}\right],\ i = 2,\ \cdots, N \tag{32c}$$

where shear stress is given by formula Eq. (22).

Presented model may also be used for an analysis of deflection and stress distribution in transversally loaded high beams (for which $/h < 10$) of homogeneous cross-section divided into N + 1 equal bending layers and N shear layers. This is an alternative for e.g. Timoshenko model. The limit case corresponding to $N \to \infty$ and $h_i, t_i \to 0$ is equivalent to the 2D equilibrium equations expressed in terms of longitudinal displacement $u(x, z)$, deflection $w(z)$ and transverse normal stress $p(x, z)$, providing that the Poisson ratio $\nu = 0$.

2.3.1. Solving the MS model governing ODEs

The system of governing equations of proposed model was numerically solved for the considered sctatical configurations with the use of author's own script based on Finite Difference Method. Total number of FDM mesh nodes is 901 what results in system of 2709 linear equations. Due to symmetry of both configurations, longitudinal displacements were assumed equal 0 in the middle of the span and free

not-loaded ends were assumed for longitudinal displacements. Concerning the boundary conditions for distribution of deflection, zero deflection and its second derivatives – namely, end-moments applied to each panel - were assumed at supported ends. Please note, that equal moments applied to all panels are independent of possible cross-sectional moment applied to the beam as a whole by applying unequal axial forces to the same panels. External point forces were applied in the form of impulse transverse load q of non-zero value only in single FDM nodes. Convergence of the proposed method was validated for two models (B-PST-3-120 and ALU-PSM-5-992– see below) – relative error is not greater than 0,005%.

2.4. Reference FEA models

Numerical calculation was also performed with the use of the Finite Element Method in Abaqus 2019 software. Fine mesh was assumed in order to provide regular shaped elements in the adhesive layers of small thickness and denser meshing in case of layers of greater thickness so that localized deformation effects could be accounted for. Point loads and point supports were accounted for as single-node boundary conditions. All models accounted for approximately 90,000 statical degrees of freedom (the number of equations in the linear system). Convergence of the estimate of system stiffness was verified for two models (B-PST-3-120 and ALU-PSM-5-992– see below) – doubling the density of mesh resulted in change of system stiffness not greater than 0,1%.

3. Experimental verification

The raw and processed data required to reproduce these findings cannot be shared at this time due to legal reasons.

3.1. Performed tests

Two statical configurations were analysed:

- Symmetric four-point bending of simply supported CLT beams – deflection was measured in the middle of the span. Statical configuration is presented in Fig. 2. Depending on specimen, beam was loaded until deflection of L/300 or L/150 was obtained.
- Symmetric three-point bending of simply supported laminated aluminium beams [25] – deflection was measured in 3 points and relative longitudinal displacement of panels' axis was measured in 4 points. Statical configuration and location of dial gauges are presented in Fig. 3. The beams was loaded in seven steps up to the value of the bending force equal 155,3N.

Figs. 4 and 5 show numerical FEA models of B-PST-3-120 and ALU-PSM-5-992 beams (see: descriptions below).

3.2. Beam types

In total 8 types of 3-panel CLT beams were analysed. Description of general form *PP-AA-t-L* has the following meaning:

- PP – panel's material
  - B – spruce wood
  - SK – plywood
  - ALU – PA-38 aluminium alloy
- AA – adhesive
  - PS – Sika ® PS polyurethane resin
  - PST – Sika ® PST polyurethane resin
  - PSM – Sika ® PSM polyurethane resin
- t – adhesive layer thickness in mm (DX means smallest possible providing adhesion)
- L – span length in mm

Dimensions h_T, h_M and h_B denote top, middle and bottom panel thickness respectively. Following types of CLT beams are considered (See Table 1).

Table 1
CLT beam types and dimensions.

LP	Description	Number of specimens	b [mm]	h_T [mm]	h_M [mm]	h_B [mm]	t [mm]	L [mm]
1	B-PS-3-120	3	100	22	25	22	3	1200
2	B-PST-3-120	3	100	22	25	22	3	1200
3	B-PST-DX-120	1	100	22	25	22	0	1200
4	B-PS-DX-120	2	100	22	25	22	0	1200
5	SK-PST-1-120	7	100	17	17	17	1	1200
6	SK-PST-1-72	6	100	17	17	17	1	720
7	SK-PST-2-120	7	100	17	17	17	2	1200
8	SK-PST-2-72	6	100	17	17	17	2	720

Following types of aluminium laminated beams are considered (See Table 2):

Table 2
Aluminium beam types and dimensions.

LP	Description	Number of specimens	b [mm]	h_T [mm]	h_B [mm]	t [mm]	L [mm]
1	ALU-PSM-5-992	1	29,25	9,656	9,656	5	992
2	ALU-PSM-3,1-992	1	29,25	9,656	9,656	3,1	992
3	ALU-PSM-1,75-992	1	29,25	9,656	9,656	1,75	992
4	ALU-PSM-1,2-992	1	29,25	9,656	9,656	1,2	992
5	ALU-PSM-0,5-992	1	29,25	9,656	9,656	0,5	992

3.3. Material characteristics

3.3.1. Spruce wood

Spruce wood was assumed an orthotropic homogeneous linear elastic solid. It's Young modulus at bending along fibres was determined in a four-point bending test on three specimens (b × h × L: 100 × 22 × 1200 mm; 120 × 38 1200 mm (two specimens)) as equal $E_{\parallel} = 11,053$ GPa. This value was assumed for edge panels with fibres along beam's axis. Ratios of this value with other elastic constants for spruce wood were estimated as average ratios for *picea sitchensis* and *picea abies* found in [26–29]. For the middle panel the Young modulus in direction transverse to fibres was assumed as an average of the values respective for radial (R) and tangential (T) directions, equal $E_{\perp} = 0,774$ GPa. Poisson ratio for middle panel was assumed as an average of ν_{RT} and ν_{TR} values equal 0,398. Poisson ratio for edge panels was assumed as an average of ν_{LR} and ν_{LT} values equal 0,452. Kirchhoff moduli we assumed equal $G_{LR} = 0,597$ GPa and $G_{RT} = 0,044$ GPa.

3.3.2. Plywood

Plywood was considered an isotropic homogeneous linear elastic solid. It's Young modulus was estimated via four-point bending test on plywood panels – the same as in SK CLT beams – as equal $E_P = 8,460$ GPa. A number of FEA tasks were performed in order to examine the influence of the value of the Poisson ratio – it was found that within the range of $\nu \in (0;0,5)$ the maximum relative change in midspan deflection was approximately 0,02%. Finally, $\nu_P = 0,3$ was assumed. Kirchhoff modulus was assumed equal $G_P = 0,600$ GPa [30].

3.3.3. PA-38 aluminium alloy

Young modulus was estimated in a simple tension test as $E_{Al} = 77,7$ GPa. Poisson ratio was assumed equal $\nu_{Al} = 0,33$.

3.3.4. Adhesives

Initial secant Young modulus for PSM resin was found in a simple tension test in ambient temperature on specimens of width 16 mm, thickness 5 mm and gauge length 45 mm with displacement rate equal 0,01 mm/s. It was found to be $E_{PSM} = 4$ MPa. Kirchhoff modulus was determined basing on assumption of incompressibility ($\nu = 0,5$) equal $G_{PSM} = 1,33$.

PS and PST resins were examined in test of simple tension of specimens of width 10 mm, thickness 4 mm and gauge length 80 mm. The specimens were seasoned for 1,5 of a month. The test was performed with three strain rate values, 0,1/min, 1/min, 10/min. Incompressible Mooney-Rivlin [31,32] model parameters were found and initial tangent moduli were then determined.

Due to fact that flexible adhesives are in fact viscous materials, strain rate was estimated for the CLT beams. Maximum shear stress τ_{max} was estimated in adhesive layers then corresponding shear strain was calculated and linear strain was determined based on principal stretch respective for simple shear deformation:

$$\varepsilon = \lambda - 1 = \frac{1}{2}(\gamma^2 + 2 + \gamma\sqrt{\gamma^2 + 4}) - 1, \quad \text{where } \gamma = \frac{\tau_{max}}{G} \tag{33}$$

Performed analysis indicated that the true strain rate in bent beams was lower than the lowest of those performed in material examination. Final values of those material parameters were taken for the lowest strain rate (See Table 3):

Table 3
Assumed material parameters of PS and PST resins.

Parameter	PS	PST
Incompressible Mooney-Rivlin: C_{01} [MPa]	8,717	2,145
Incompressible Mooney-Rivlin: C_{10} [MPa]	−4,878	−0,118
Initial tangent Kirchhoff modulus: $G_0 = 2(C_{01} + C_{10})$ [MPa]	7,678	4,054
Initial tangent Young modulus: $E_0 = 3G_0$ [MPa]	23,034	12,162

3.4. Comparison of results

System stiffness, defined as ratio between load and maximum deflection, was calculated for each model and compared with the experiment-based stiffness, estimated as a slope of a linear regression. In case of CLT beams the set of experimental data for which regression was calculated was limited to those values for which the stress–strain curve was constantly convex in order to neglect load process initialization disturbances. Last experimental data point was either the one corresponding with L/300 deflection, or the peak value before unloading. In case of the aluminium laminate beams the regression was calculated basing on 7 experimental data point corresponding with performed load steps.

Estimation of system stiffness for a three-point bending test of a simply supported beam according to Bernoulli-Euler model is:

$$k = \left[\frac{23}{1296}\frac{L^3}{D_b}\right]^{-1} \tag{34}$$

and for Timoshenko model:

$$k = \left[\frac{23}{1296}\frac{L^3}{D_b} + \frac{L}{6\kappa D_s}\right]^{-1} \tag{35}$$

Estimation of system stiffness for a four-point bending test of a simply supported beam according to Bernoulli-Euler model is:

$$k = \left[\frac{1}{48}\frac{L^3}{D_b}\right]^{-1} \tag{36}$$

and for Timoshenko model:

$$k = \left[\frac{1}{48}\frac{L^3}{D_b} + \frac{L}{4\kappa D_s}\right]^{-1} \tag{37}$$

The comparison of obtained results for the CLT beams under four-point bending are presented in Fig. 6 and in Table 4. MS estimate for zero-thickness adhesive layer are not presented as the Eqs. (23) to (26) are no longer valid for $t_i = 0$ and numerical calculations diverge as $t_i \to 0$.

Load displacement curves for 3 specimens of SK-PST-1-72 beam, as well as theoretical and numerical predictions of linear deformation according to considered model are presented in Fig. 7.

Strain was not measured during the deformation, so no experimental verification of the strain or stress estimate can be performed. However numerical estimates for each model can be carried out and the results are close one to another – they are shown Figs. 8–10 and Tables 5–7. Maximum normal stress in case of FEA is located in the neighbourhood of the point of application of external load and it is greater

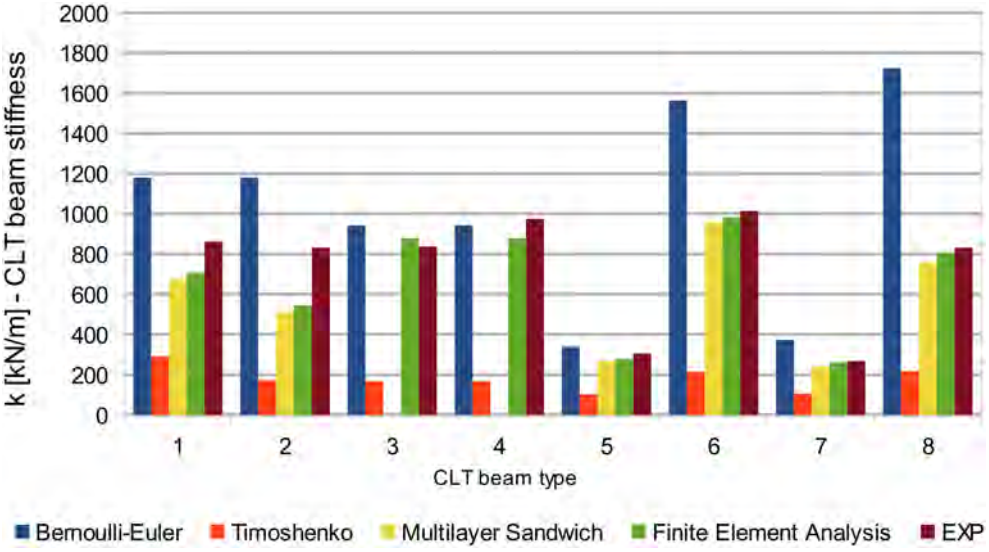

Fig. 6. Comparison of calculated system stiffness for considered models with experimental results for CLT beams.

Table 4
Estimated and measured stiffness of CLT beams.

Beam	System stiffness k [kN/m]								
	Bernoulli-Euler	BE/EXP	Timoshenko	T/EXP	Multilayer Sandwich	MS/EXP	Finite Element Analysis	FEA/EXP	EXP
B-PS-3-120	1181,01	137,06%	289,97	33,65%	671,24	77,90%	706,95	82,04%	861,70
B-PST-3-120	1180,97	142,06%	173,70	20,89%	513,74	61,80%	544,07	65,45%	831,32
B-PST-DX-120	943,04	112,53%	167,56	20,00%	–	–	877,48	104,71%	838,00
B-PS-DX-120	943,04	96,71%	167,56	17,18%	–	–	877,48	89,99%	975,08
SK-PST-1-120	337,79	110,80%	103,01	33,79%	266,15	87,30%	277,77	91,11%	304,87
SK-PST-1-72	1563,83	154,22%	213,31	21,04%	955,9	94,27%	980,20	96,67%	1014,00
SK-PST-2-120	372,50	139,76%	106,52	39,97%	239,25	89,77%	261,09	97,96%	266,52
SK-PST-2-72	1724,54	207,27%	217,29	26,12%	757,72	91,07%	807,17	97,01%	832,03

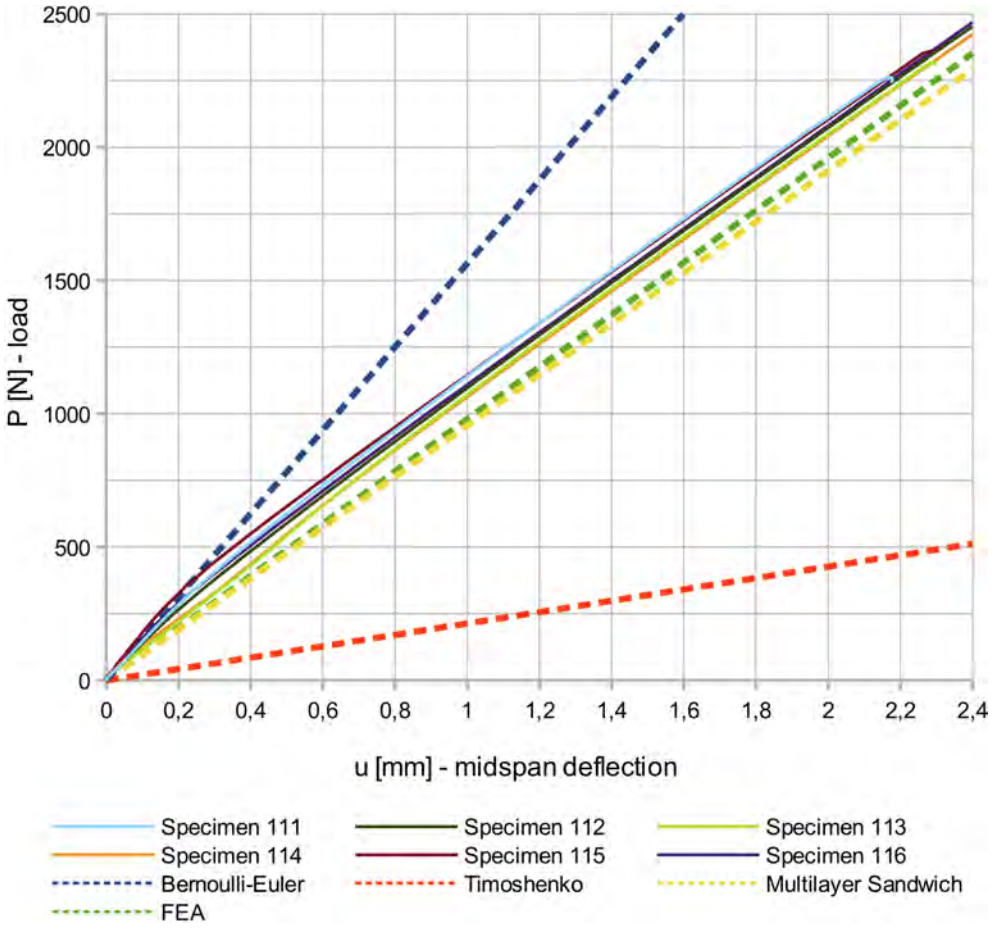

Fig. 7. Force-displacement curves for 6 specimens of the B-PST-3-120 beam and theoretical predictions of the system stiffness.

than the normal stress in the middle of the span due to local effects caused by point load.

The comparison of obtained results for the aluminium laminated beams under three-point bending are presented in Fig. 11 and Table 8.

Relative longitudinal displacements of aluminium panels axes are plotted in Figs. 12 and 13 for two thicknesses of adhesive layer. It can be seen that for a thin adhesive layer the predictions of MS model and FEA are qualitatively the same as the observed deformations, yet quantitative estimate is not precise. However, for adhesive layers of greater thickness both models underestimate the true displacement – the thicker the layer, the greater discrepancy with experimental results.

4. Conclusions and discussion of results

It can be noticed that in general:

- BE model overestimates the system stiffness,
- T model underestimates the system stiffness,
- FEA and MS models slightly underestimate the system stiffness,
- FEA and MS models are in good accordance with each other,
- MS model predicts higher values of maximum normal stress than other models,
- Estimation of maximum shear stress in the middle of bent panels

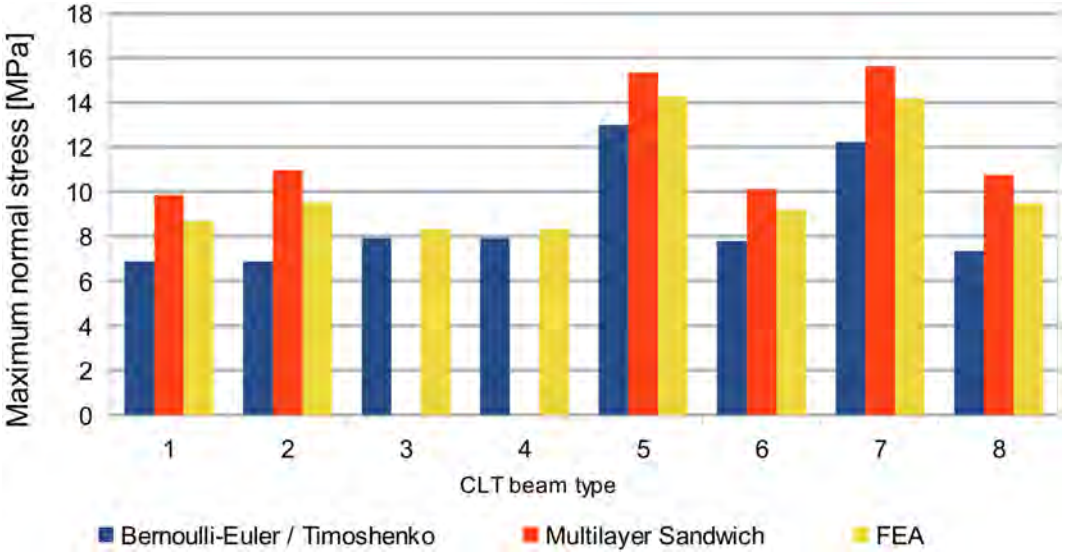

Fig. 8. Comparison of estimates of maximum normal stress for CLT beam models.

with the use of Zhuravsky theory applied to MS and BE/T models gives smaller values than those predicted in FEA,

- Estimation of shear stress in adhesive layer is approximately the same in all models.

Large discrepancy between BE and T model estimates and experimental results are due to violation of a fundamental assumption of these models on lack of deplanation. It can be easily shown that adhesive layers are strongly sheared and the panels are displaced one with respect to another (see: Fig. 14).

The reason for which T model gives such strong underestimate and it differs so much from the BE model estimate is the unusual small value of the shear correction factor. The normal stress distribution, on which the function $s(z)$ is based in Eq. (10), makes the numerator of integrand bell-shaped in such a way that only the values of $G(z)$ which are close to the weighted centroid make a considerable contribution to the value of the integral. In case of all considered beams those values are relatively small and placed in denominator making the final value of integral large and its reciprocal – the shear correction factor – small. Due to invalid assumption on deformation of cross-section, improper normal stress distribution resulting from that assumption decrease the contribution of the most rigid edge panels to the overall shear rigidity strongly overestimating the systems shear compliance. However, the estimate of the shear correction factor given by Eq. (10) can still be useful if only those basic assumptions are approximately fulfilled – it can be shown that for very thin adhesive layer (ALU beam 5, in which $t/h \approx 0,05$) system stiffness predicted by the Timoshenko beam model is close to estimates of MS model and FEA, approximately 80% of the value obtained in experiment (See Fig. 15).

Considering slight underestimate of the MS model with respect to

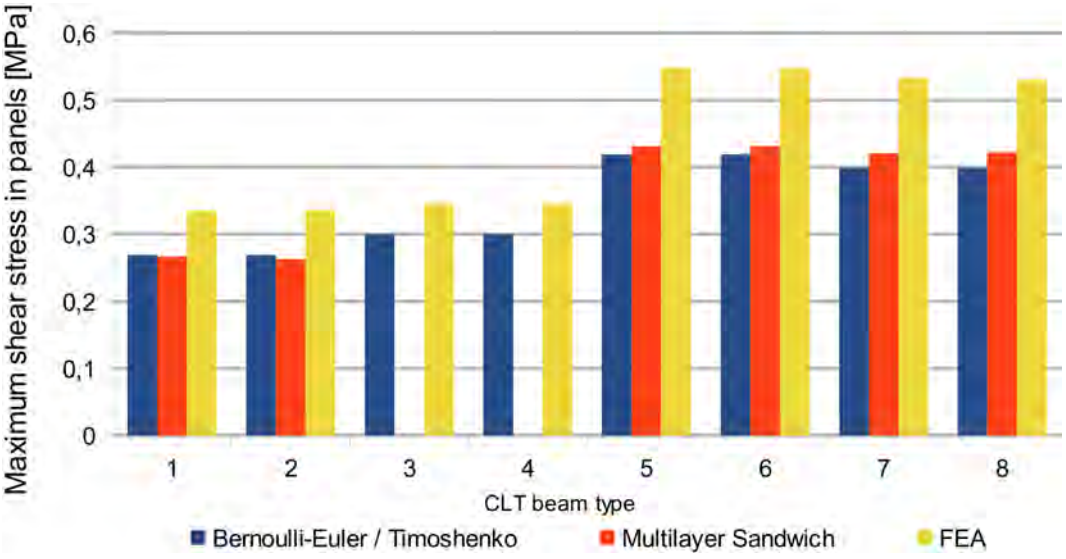

Fig. 9. Comparison of estimates of maximum shear stress in adhesive for CLT beam models.

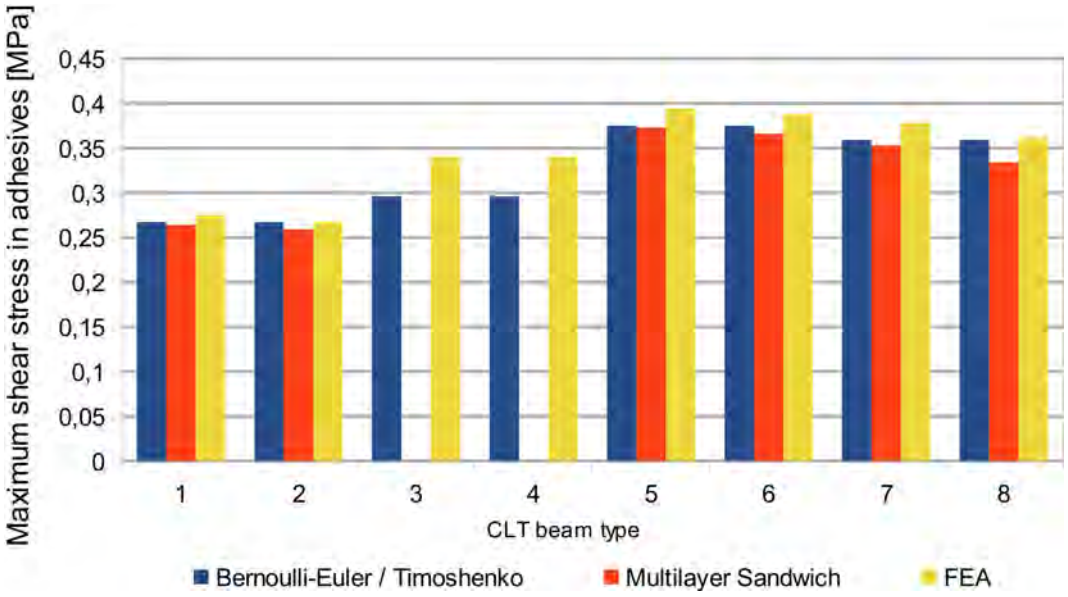

Fig. 10. Comparison of estimates of maximum shear stress in bent panels for CLT beam models.

Table 5
Estimates of maximum normal stress in panels of CLT beams.

Beam	Estimate of maximum normal stress in panels [MPa]		
	Bernoulli-Euler/Timoshenko	Multilayer sandwich	FEA
B-PS-3-120	6,867	9,850	8,678
B-PST-3-120	6,867	10,958	9,530
B-PST-DX-120	7,911	–	8,330
B-PS-DX-120	7,911	–	8,330
SK-PST-1-120	12,985	15,341	14,279
SK-PST-1-72	7,791	10,113	9,176
SK-PST-2-120	12,220	15,632	14,173
SK-PST-2-72	7,332	10,755	9,485

Table 6
Estimates of maximum shear stress in panels of CLT beams.

Beam	Estimate of maximum shear stress in panels [MPa]		
	Bernoulli-Euler/Timoshenko	Multilayer Sandwich	FEA
B-PS-3-120	0,269	0,267	0,335
B-PST-3-120	0,269	0,263	0,336
B-PST-DX-120	0,300	–	0,346
B-PS-DX-120	0,300	–	0,346
SK-PST-1-120	0,419	0,431	0,548
SK-PST-1-72	0,419	0,431	0,547
SK-PST-2-120	0,399	0,421	0,533
SK-PST-2-72	0,399	0,422	0,531

Table 7
Estimates of maximum shear stress in adhesives of CLT beams.

Beam	Estimate of maximum shear stress in adhesives [MPa]		
	Bernoulli-Euler/Timoshenko	Multilayer sandwich	FEA
B-PS-3-120	0,267	0,264	0,275
B-PST-3-120	0,267	0,259	0,268
B-PST-DX-120	0,296	–	0,340
B-PS-DX-120	0,296	–	0,340
SK-PST-1-120	0,375	0,373	0,395
SK-PST-1-72	0,375	0,366	0,388
SK-PST-2-120	0,359	0,353	0,378
SK-PST-2-72	0,359	0,334	0,362

experimental data and FEA results, it should be noted that axial strain of a shear layer is neglected. In fact, a linear distribution of longitudinal displacements in shear layer with non-zero average value requires a non-zero axial force in such a layer – this is depicted in a simplified way in Fig. 16. Any change in such a force along beam's axis could be equilibrated only by a through-the-thickness change in shear stress which is assumed to be zero. Thus, the axial force in shear layer must be constant along beam's axis what is contrary to the assumption that longitudinal displacements of bending layers are in general functions of x. It is clear that simple kinematics assumed for the shear layers is only an approximation. Neglecting axial stiffness of the shear layers is one of the reasons for which the MS model provide an underestimated system stiffness.

Another reason for this underestimate is neglecting the transverse deformation, namely contraction due to transverse normal stress caused by applied load. In the MS model work of external forces is completely transformed into strain energy of shear, elongation and bending, while in true deformation part of it is transformed into transverse linear strain, especially in the neighbourhood of external point forces. It is obvious that point force applied to top panel causes local deformation in beam resulting in smaller deflection (thus, greater system stiffness) of bottom panel, where the measurement is performed. Those features of deformation cannot be observed with an unaided eye even in case of highly deformed beam (Fig. 16) – they are depicted in an exaggerated way in Fig. 17.

Proposed MS model is in good accordance in precise (fine mesh) FEM analysis – in case of all considered beams, the MS model estimates were 90%-98% of the FEA estimate of system stiffness. Such an estimate was obtained by solving a problem of much smaller computational size – the MS model consisted of system of at most 2709 equations (for three-panel beam), while FE model had more than 90,000 equations. Another benefit due to use of simplified one-dimensional model is the lack of any meshing issues, as for the FDM a uniform discretization of a single dimension is sufficient to obtain the result. It is obvious that FEA do not require such a dense mesh as the one used, however any attempt for reduction of number of equations must account for the fact, that large FE sizes in panels may lead to insufficient number of through-the-thickness elements or ill-shaped elements in adhesive layers of much smaller dimensions unless different meshing is used for those layers. Those issues contribute to the overall computational effort and time in favour of MS model.

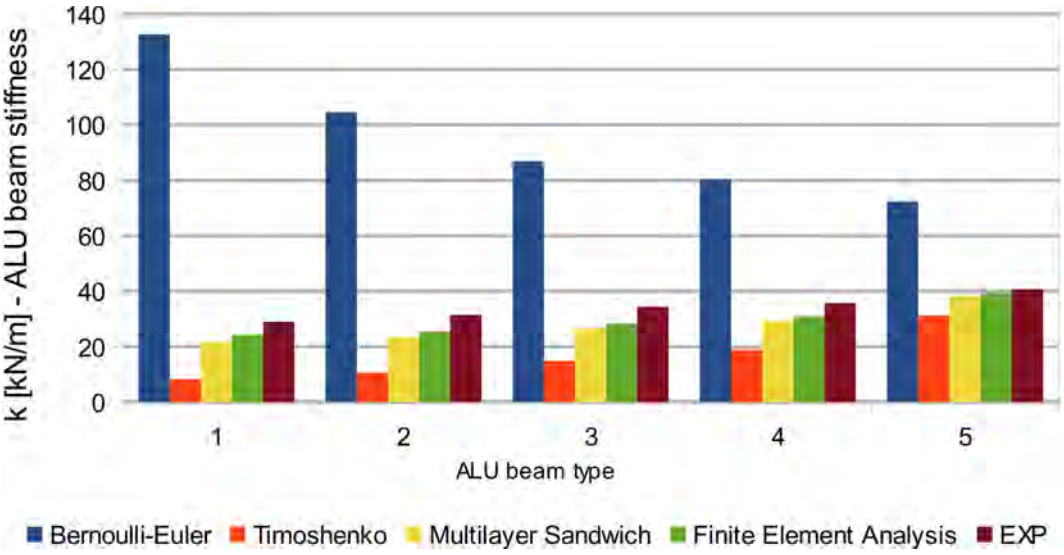

Fig. 11. Comparison of calculated system stiffness for considered models with experimental results for aluminium beams.

Table 8
Estimated and measured stiffness of ALU beams.

Beam	System stiffness k [kN/m]								
	Bernoulli-Euler	BE/EXP	Timoshenko	T/EXP	Multilayer Sandwich	MS/EXP	Finite Element Analysis	FEA/EXP	EXP
ALU-PSM-5-992	132,660	457,97%	8,296	28,64%	21,739	75,05%	24,202	83,55%	28,967
ALU-PSM-3,1-992	104,560	332,87%	10,526	33,51%	23,468	74,71%	25,523	81,25%	31,412
ALU-PSM-1,75-992	86,960	252,64%	14,868	43,20%	26,588	77,25%	28,278	82,15%	34,42
ALU-PSM-1,2-992	80,354	225,09%	18,863	52,84%	29,411	82,39%	30,887	86,52%	35,699
ALU-PSM-0,5-992	72,419	177,97%	31,218	76,72%	38,311	94,15%	39,234	96,42%	40,691

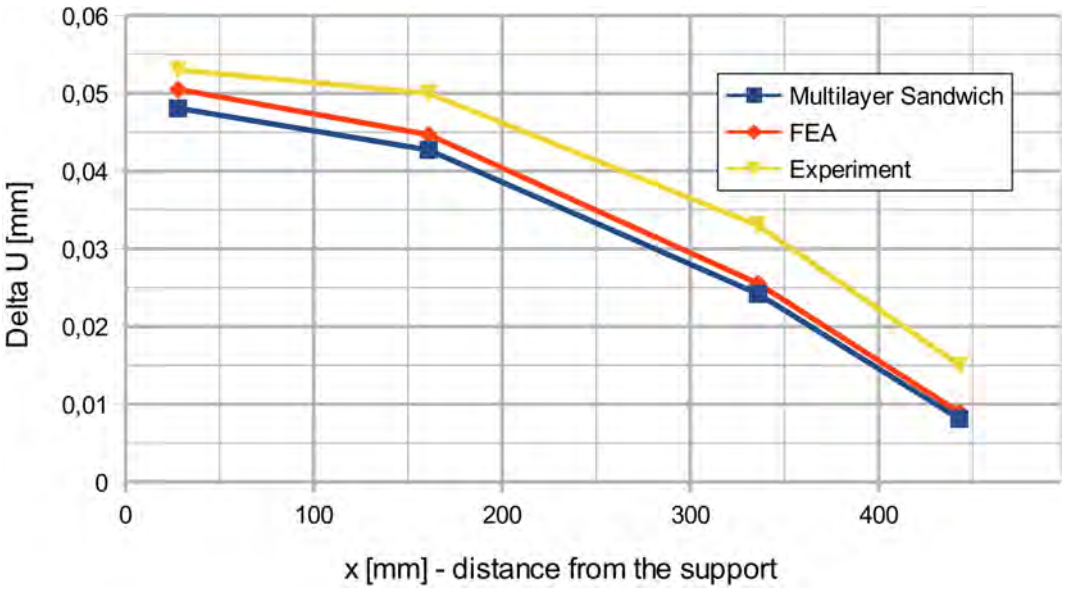

Fig. 12. Relative axial displacement of panels of ALU-PSM-0,5-992 beam type. Comparison of numerical estimates and experimental data.

5. Summary

Three one-dimensional linear elastic models of multi-layer composite beams were compared with 2D Finite Element Analysis results and experimental data corresponding with 8 beam types in three-point bending and 5 beam types in four-point bending. A system of governing equations for a multi-layer sandwich beam was derived. An estimation for the shear correction factor for composite Timoshenko beams was proposed. While classical models of Bernoulli-Euler and Timoshenko provide poor estimate of global system stiffness, proposed multi-layer sandwich model is in good accordance with FEA results and experimental data. Stress distribution is predicted in a similar manner by all models, with MS slightly overestimating (wrt FEA) the maximum normal stress and all one-dimensional models underestimating (wrt FEA) the maximum shear stress in bent panels.

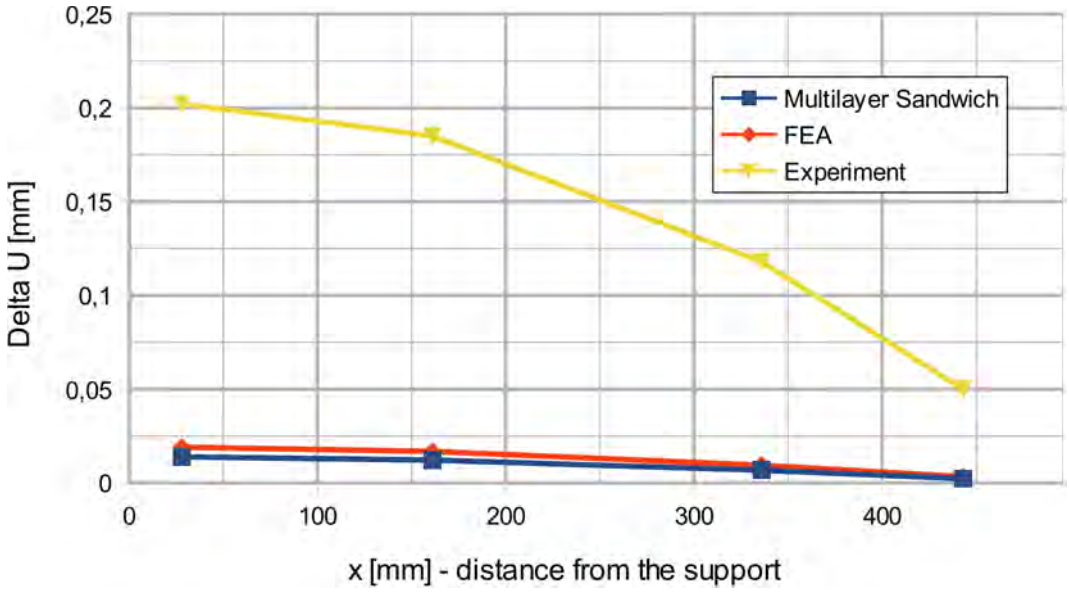

Fig. 13. Relative axial displacement of panels of ALU-PSM-5-992 beam type. Comparison of numerical estimates and experimental data.

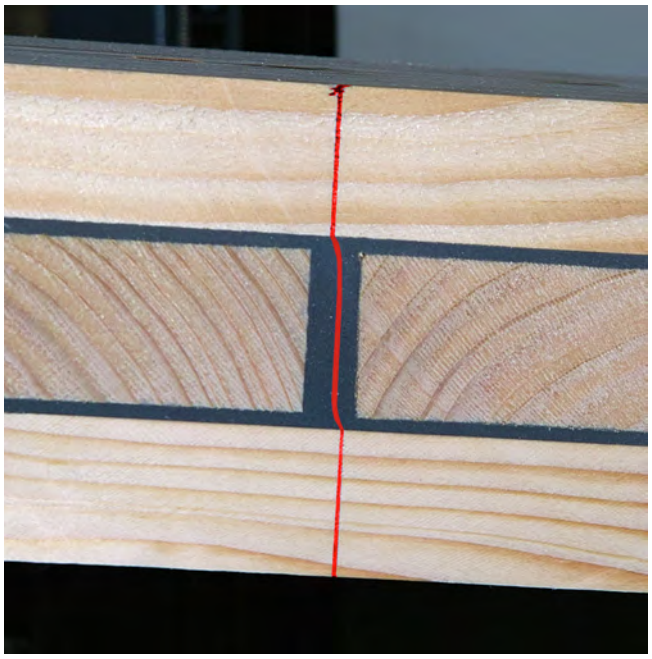

Fig. 14. Deplanation of cross-section due to relative displacements of bent panels.

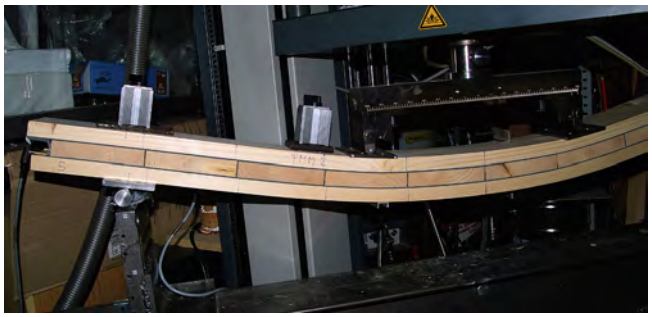

Fig. 15. CLT beam specimen undergoing large deformation.

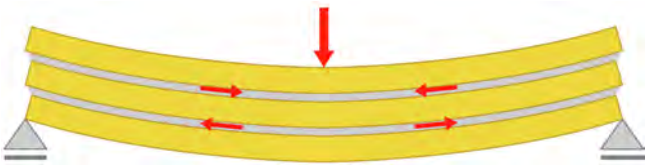

Fig. 16. Axial deformation of shear layers.

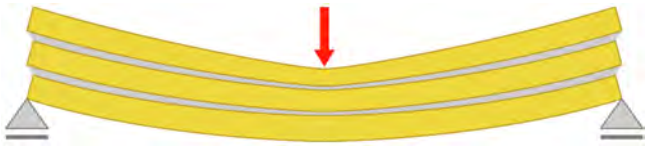

Fig. 17. Through-the-thickness deformation of the beam.

Declaration of Competing Interest

The authors declare that they have no known competing financial interests or personal relationships that could have appeared to influence the work reported in this paper.

Acknowledgement

I would like to thank dr hab. A. Kwiecień, prof. PK, and dr B. Zając from the Cracow University of Technology for making their experimental results available to me, what enabled me to perform validation of analysed models. I would like to give special thanks to dr Marcin Nowak from Institute of Fundamental Technological Research of Polish Academy of Sciences for his aid in performing FEM analysis.

Author acknowledge the financial support of experimental research from the project No POIR.01.01.01-00-0828/16, realized in Poland by the company PalettenWerk Kozik Sp. J.

Data availability statement

The raw and processed data required to reproduce these findings cannot be shared at this time due to legal reasons.

Appendix A. Supplementary data

Supplementary data to this article can be found online at https://doi.org/10.1016/j.compstruct.2020.112088.

References

[1] Kwiecień A. Stiff and flexible adhesives bonding CFRP to masonry substrates-Investigated in pull-off test and Single-Lap test. Arch Civ Mech Eng 2012;12:228–39. https://doi.org/10.1016/j.acme.2012.03.015.

[2] Kwiecień A. Shear bond of composites-to-brick applied with highly deformable, in relation to resin epoxy, interface materials. Mater Struct Constr 2014;47:2005–20. https://doi.org/10.1617/s11527-014-0363-y.

[3] Kwiecień A, de Felice G, Oliveira DV, Zając B, Bellini A, De Santis S, et al. Repair of composite-to-masonry bond using flexible matrix. Mater Struct Constr 2016;49:2563–80. https://doi.org/10.1617/s11527-015-0668-5.

[4] Carrera E, Petrolo M. Refined One-Dimensional Formulations for Laminated Structure Analysis. AIAA J 2012;50:176–89.

[5] Timoshenko SP, Gere JM. Mechanics of materials. Secon Edit. Boston: PWS-KENT Publishing Company; 1984.

[6] Plantema FJ. Sandwich construction: the bending and buckling of sandwich beams, plates, and shells. New York: Jon Wiley and Sons; 1966.

[7] Touratier M. An efficient standard plate theory. Int J Eng Sci 1991;29:901–16.

[8] Reddy JN. A simple higher-order theory for laminated composite plates. J Appl Mech 1984;51:745–52.

[9] Vo TP, Thai HT, Nguyen TK, Inam F, Lee J. Static behaviour of functionally graded sandwich beams using a quasi-3D theory. Compos Part B Eng 2015;68:59–74. https://doi.org/10.1016/j.compositesb.2014.08.030.

[10] Catapano A, Giunta G, Belouettar S, Carrera E. Static analysis of laminated beams via a unified formulation. Compos Struct 2011;94:75–83. https://doi.org/10.1016/j.compstruct.2011.07.015.

[11] Vo TP, Thai HT, Nguyen TK, Lanc D, Karamanli A. Flexural analysis of laminated composite and sandwich beams using a four-unknown shear and normal deformation theory. Compos Struct 2017;176:388–97. https://doi.org/10.1016/j.compstruct.2017.05.041.

[12] Vo TP, Thai HT. Static behavior of composite beams using various refined shear deformation theories. Compos Struct 2012;94:2513–22. https://doi.org/10.1016/j.compstruct.2012.02.010.

[13] Zhuravsky DI. Sur la résistance d'un corps prismatique et d'une pièce composée en bois ou en tôle de fer à une force perpendiculaire à leur longueur. Mémoires Ann Des Ponts Chaussées 1856;2:328–51.

[14] Love AEH. A treatise on the mathematical theory of elasticity. Second Edi. Cambridge: Cambridge University Press; 1906.

[15] Dong SB, Alpdogan C, Taciroglu E. Much ado about shear correction factors in Timoshenko beam theory. Int J Solids Struct 2010;47:1651–65. https://doi.org/10.1016/j.ijsolstr.2010.02.018.

[16] Chan KT, Lai KF, Stephen NG, Young K. A new method to determine the shear coefficient of Timoshenko beam theory. J Sound Vib 2011;330:3488–97. https://doi.org/10.1016/j.jsv.2011.02.012.

[17] Dong SB, Çarbaş S, Taciroglu E. On principal shear axes for correction factors in Timoshenko beam theory. Int J Solids Struct 2013;50:1681–8. https://doi.org/10.1016/j.ijsolstr.2013.01.034.

[18] Kaneko T, Rosinger HE, Ritchie IG, Hardie D, Parkins RN. Applied physics related content on timoshenko ' s correction for shear in vibrating beams on timoshenko ' s correction for shear in vibrating beams. J Phys D Appl Phys 1975;8:1927–36.

[19] Gruttmann F. Shear correction factors in Timoshenko ' s beam theory for arbitrary shaped cross – sections 2001;27:1–20.

[20] Marinetti A, Oliveto G. On the Evaluation of the Shear Correction Factors: a Boundary Element Approach n.d.

[21] Tsai MY, Oplinger DW, Morton J. Tsai_model złącza.pdf. Int J Solids Struct 1998;35:1163–85.

[22] de Bruyne NA. The Strength of glued joints. Aircr Eng 1944;16:115–8.

[23] Goland M, Reissner E. J Appl Mech 1944;11:A17–27.

[24] Volkersen O. Die Nietkraftverteilung in zugbeanspruchten Nietverbindungen mit konstanten Laschenquerschnitten. Luftfahrtforshung 1938;15:41–7.

[25] Zając B. Doświadczalno-analityczne określenie wytężenia polimerowej skleiny w belkach zespolonych. Cracow University of Technology, 2008.

[26] Keunecke D, Sonderegger W, Pereteanu K, Lüthi T, Niemz P. Determination of Young's and shear moduli of common yew and Norway spruce by means of ultrasonic waves. Wood Sci Technol 2007;41:309–27. https://doi.org/10.1007/s00226-006-0107-4.

[27] Dumond P, Baddour N. Mechanical property relationships in sitka spruce soundboard wood. Int Conf Noise Vib Eng ISMA 2014.

[28] Kretschmann DE, editor. Wood Handbook. Wood as an Engineering Material. Madison, Wisconsis: Forest Products Laboratory, Forest Service; 2010.

[29] Neuhaus H. Elastizitaetszahlen von Fichtenholz in Abhaengigkeit von der Holzfeuchtigkeit. Ruhr-Universitaet Bochum 1981.

[30] Möhler K. Grundlagen der Holz-Hochbaukonstruktionen. In: Götz K-H, Hoor D, Möhler K, Natterer J, editors. Holzbau-Atlas, München: Institut für internationale Architektur-Dokumentation; 1980.

[31] Mooney M. A theory of large elastic deformation. J Appl Phys 1940;11:582–92.

[32] Rivlin RS. Large elastic deformations of isotropic materials. IV. Further developments of the general theory. Philos Trans R Soc London Ser A Math Phys Sci 1948;241:379–97.